ECS Transactions, 3 (25) 317-327 (2007)
10.1149/1.2753264, copyright The Electrochemical Society

Fabrication and Operation of Magnetic Quantum-Dot Cellular Automata All Magnetic Logic

A. Orlov[a], A. Imre[b], L. Ji[a], G. Csaba[c], G. H. Bernstein[a], and W. Porod[a]

[a] University of Notre Dame, Center for Nano Science and Technology, Notre Dame, IN 46556, USA
[b] Argonne National Laboratory, Materials Science Division and Center for Nanoscale Materials, Argonne, IL 60439, USA
[c] Technical University of Munich, Institute for Nanoelectronics, Munich, D-80333, Germany

We report the fabrication of, and demonstrate logic functionality in, networks of magnetically-coupled, nanometer-scale magnets performing binary computation in a Magnetic Quantum-dot Cellular Automata (MQCA) system. MQCA is an all-magnetic logic that offers low power dissipation and high integration density of functional elements. Basic elements of MQCA architecture such as binary wire, three input majority logic gate, and a combination of the two logic elements are demonstrated at room temperature.

Introduction

Recent discoveries in the field of magnetic sensors and developments in manufacturing high quality magnetic films have lead to the rapid development of magnetic storage devices and an ever-increasing density of information storage. Despite this tremendous success in magnetic data storage, there have been relatively few attempts to exploit magnetic phenomena for logic (1-5). This is primarily caused by the continuing progress of the CMOS- paradigm based on field-effect transistors. However, the use of all-magnetic logic devices could be beneficial as compared to the CMOS in a variety of applications. Applications for all-magnetic logic include power failure insensitive logic, ultra-low-power applications, computing in radiation-hard environments, or architectures incorporating magnetic random access memory (MRAM).

One of the possible architectures suitable for building logic using nanomagnets is the Quantum-dot Cellular Automata (QCA) signal processing approach (6). In QCA architecture binary logic is built from simple, nominally identical, bistable units that are locally connected to each other solely by electromagnetic forces; consequently, the signal processing function is defined by the physical placement of the building blocks that constitute the computing architecture (7-9). The QCA concept can be realized in different physical systems. It was originally proposed to use electrostatically-coupled arrays of quantum dots employing the Coulomb-blockade phenomenon to perform binary operations (6). The first functional electronic QCA (EQCA) cell was experimentally demonstrated (10) in 1997, followed by the logic gate (11), and the shift register (12). Micron-sized metal (Al) dots separated by small (50×50 nm^2) oxide tunnel junctions were used in these experiments, which were performed at sub-Kelvin temperatures due to the small energy difference between the ground and excited states, so called "kink" energy. With this EQCA embodiment (13) the value of kink energy is only about $1K\times k_B$ (k_B is

Boltzmann's constant). Room temperature EQCA can be achieved only for the size of a cell reduced to molecular scale (14,15), the technology for which has not yet been demonstrated. Another fundamental difficulty in realization of EQCA is the necessity to counterbalance the random background charge – a problem for which a solution has not yet been proposed.

Luckily, the QCA computational paradigm can be applied to arrays of coupled nanomagnets where information is represented by polarization of magnetic domains. We refer to this class of devices as magnetic QCA, or MQCA[1]. In MQCA the cells comprise single-domain magnets on the size scale of 10 – 100 nm (above the superparamagnetic limit, but within the single-domain limit), and are expected to operate at room temperature because of the much larger kink energies (on the order of $5000K \times k_B$) (5,15). As the building blocks for MQCA we chose the elongated single-domain magnets similar in shape and magnetic state to the larger magnets in the one-domain state (Fig. 1). The planar nanomagnets were fabricated on oxidized silicon wafers. For patterning, electron-beam lithography followed by e-beam deposition of 30 nm permalloy (NiFe) film and lift-off were used.

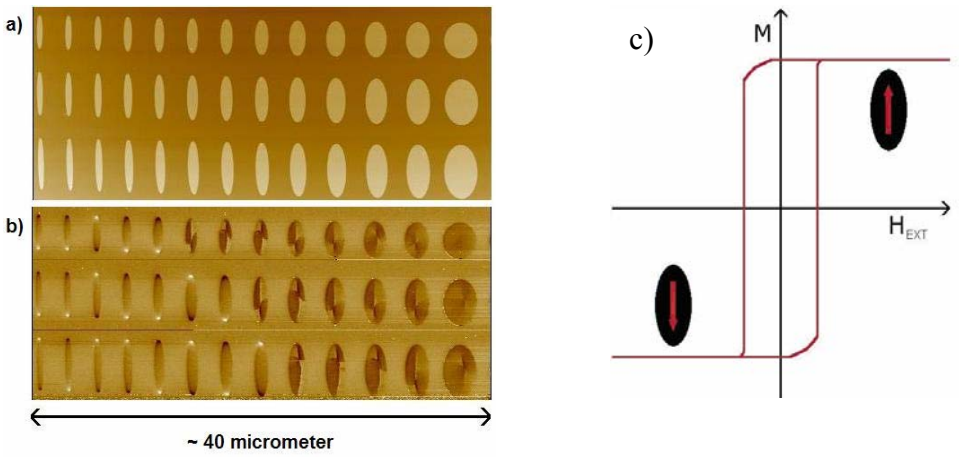

Figure 1. Magnetic states of patterned ferromagnetic elements. (a) Topographic atomic force microscope (AFM) image of thin-film, polycrystalline NiFe magnetic elements in a row, made by electron-beam lithography and lift-off. While the height of the oval elements in each row is kept the same, the width is varied. (b) MFM image of remanent magnetization. Strong contrast in the MFM images of one-domain magnets (c) Two magnetizations of nanomagnets representing two binary states of MQCA.

[1] Cowburn et al. (2) describes the realization of magnetic QCA (MQCA) operation in chains of 110 nm diameter disk-shaped magnetic particles that manifest collective behavior. In this system, the preferred magnetization direction of the disks (the representation of binary information) as well as the magnetization reversal process (the information propagation) are primarily determined by coupling-induced magnetic anisotropy in the chains. Our approach to MQCA is similar, but we employ an additional shape-induced anisotropy component to separate the directions for magnetic information representation and information propagation in the array (5).

The submicron elongated single-domain magnets are strongly bistable, as their remanent magnetization (magnetization at zero external field) always points along their long axis due to shape-induced magnetic anisotropy (Fig. 1c). Even though a magnetizing force can temporarily rotate the magnetization away from the long axis, the magnet relaxes to either of the two remanent states when the force is removed. The process of temporarily magnetizing perpendicular to the long axis can be pictured as the magnetizing force pulling down and then releasing the energy barrier between the remanent ground states.

For the one-domain state, unlike the two-domain or vortex configurations (also shown in Fig. 1b), the magnetic flux lines close outside of the magnets, creating strong magnetic stray fields that can be used to couple elements in close proximity through dipole-dipole interactions. The resulting magnetization pattern for an array of nanomagnets depends on their spatial physical arrangement. For example, arranging several of these magnets to be collinear along their long axes results in a line of magnets favoring their magnetization to point in the same direction, i.e. the ferromagnetically-ordered state. Placing them side-by-side and parallel to each other results in a line that favors antiparallel alignment of the magnetic dipoles, i.e. the antiferromagnetically-ordered state. In MQCA, these coupling-induced ordering phenomena are used to drive the computation.

A very important issue for the proper operation of QCA-based systems is the presence of a clocking field (electrical for EQCA, and magnetic for MQCA) that ensures the correct switching of logic gates into their ground state. This field acts as an additional source of energy (on top of the energy supplied by the input), similar to a power supply for conventional electronics and allows the logic level restoration, power gain and prevents the QCA system from being trapped in an undesirable metastable state (17). For MQCA this can be achieved by applying an external clocking field along the hard axis of the magnets that puts them into a logically neutral state (erases their memory); further slow reduction of the clocking field to zero brings the magnetic system to its ground state, which in turn depends on the polarization of the input magnets. Clocking has other benefits as well: it can be used to realize pipelined circuits and ensure that signals propagate from the inputs toward the outputs and not the other way round (9).

Demonstration of Binary Wire for MQCA

Let us consider first the lines of antiferromagnetically coupled (AFC) nanomagnets in the oriented vertically (in the Y direction) representing binary wires (Fig. 2). The horizontally oriented (elongated along the X axis) nanomagnets in the right hand side and the left hand side of each binary wire are used as inputs to set the state of the linear array.

In the absence of these input magnets the ground state of the antiferromagnetically-coupled line could be one of two possible complementary alternating dipole configurations (either up-down-up-down-etc. or down-up-down-up-etc.) Setting the state of the input magnet by an external field in the x-direction breaks this symmetry and favors one of the two possible complementary states of the line. The clocking field for such a binary wire is oriented horizontally (along X direction). The effect of such a horizontal field on the vertical dots is to add an X-component of magnetization to the preferred Y-direction. For sufficiently strong clocking fields (typically several hundred

Oe), the magnetization vectors of all nanomagnets in the line can be forced to point in the X-direction, but this state will persist only so long as the clocking field is maintained, and the nanomagnets will return to their preferred state with magnetization in the Y-direction upon removal of this field. The crucial point here is that this switching behavior from magnetization in the X-direction to either up or down magnetization in the Y-direction is strongly influenced by any additional fields, such as coupling fields from either the

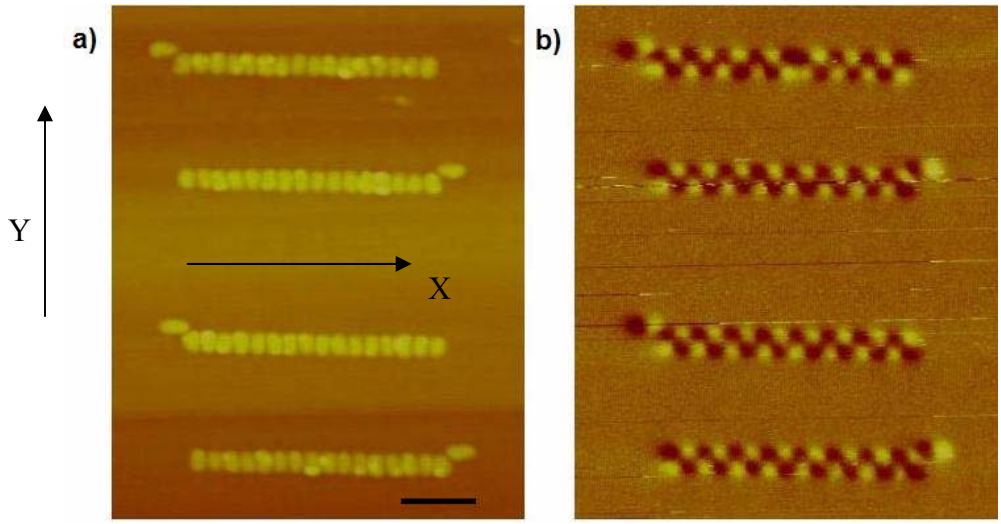

Figure 2. Antiferromagnetic ordering in a line of nanomagnets. The ordering along the chain is controlled by an additional, horizontally-oriented elongated driver magnets. (a) AFM image of nanomagnets. (b) MFM image of the same chain shows alternating magnetization of the magnets as set by the state of the horizontal driver magnets. Scaling bar length is 500 nm.

neighbors or the input magnet. The effect of the magnetic field for such arrangements of the binary wire and input magnets is two-folded: first, it acts as a clocking field in the X-direction in order to place the line of coupled magnets into an intermediate state, and second, it sets the magnetization of the input magnets placed orthogonal to the wire. The magnetic fringe fields from the input nanomagnets then determine which ground-state configuration the array assumes after removal of the clocking field. We have studied this switching behavior both through extensive micromagnetic simulations (16), and observed it experimentally. It can be seen that from Fig. 2 that the binary wire assumes the configuration suggested by the input nanomagnets. An error in the top binary wire in Fig. 2b most likely is caused by the fabrication defect.

Demonstration of a majority gate for MQCA

Figure 3 shows a physical layout, schematic representation, and a truth table for the key element of MQCA logic – the majority gate. The nanomagnets are arranged along two intersecting lines, where the dipole coupling of the nanomagnets produces ferromagnetic ordering along the vertical line and antiferromagnetic ordering along the horizontal line. This structure is similar to that proposed in (17) (and also studied in (18)), except that we consider the output of the gate to be in the AFC line instead of the FC line.

Consider the simplest arrangement of five nanomagnets, i.e. a central nanomagnet surrounded by four others (Fig. 4a). Three of the neighbors (A, B, C in Fig. 4a) can be used as inputs driven by additional driver nanomagnets oriented in the x-direction, labeled D, along the clocking field. The fourth neighbour (OUT), to the right of the central magnet in Fig. 4a, is the output. Our gate is constructed so that the ferromagnetic and antiferromagnetic coupling to the central nanomagnet have the same strength, and therefore it switches to the state to which the majority of inputs forces it. In a real world application the driver magnets must be driven by external input signals,

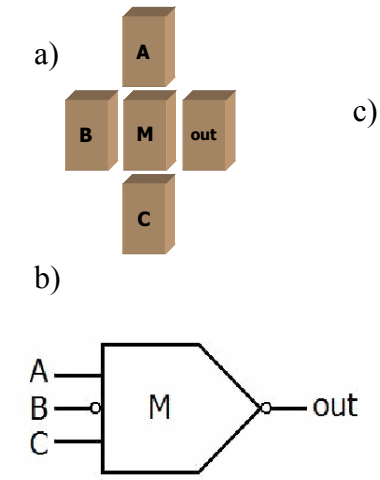

c)

A	B	C	$A\bar{B}C$	M	out	
0	0	0	010	0	1	
0	0	1	011	1	0	if B=0 then out=NOR(A,C)
1	0	0	110	1	0	
1	0	1	111	1	0	
0	1	0	000	0	1	
0	1	1	001	0	1	if B=1 then out=NAND(A,C)
1	1	0	100	0	1	
1	1	1	101	1	0	

Figure 3. Physical layout (a), schematic representation (b), and the truth table (c) for MQCA majority gate. Note that input B, and output are inverted. Decision is made based on the majority voting.

schematically represented by magnetic field lines in Fig. 4a. One of the obstacles for MQCA realization is the difficulty of local coupling of external signals to the nanomagnets: at the moment we do not have the inputs to switch the drivers independently. However, for the sake of the majority logic gate demonstration, all possible eight input logic combinations can be tested, by fabricating four structures with different spatial location of the driver nanomagnets (Fig. 4b).

Simulations (20) of the magnetic states of the majority gates after applying a horizontal clocking field show that as the clocking field falls, switching inside the gate begins at the input magnets and ends at the output magnet. We successfully demonstrated the operation of the majority gate (21). Our investigations demonstrate that correct operation of the majority-gate structure (with no errors in the final state imposed by the drivers) occurs with the probability of about 0.25 when the applied clocking field was aligned with the horizontal axis with approximately ± 1° accuracy. For comparison, the probability of all eight nanomagnets randomly assuming the correct orientation is less than 0.004. The fact that we observed a much larger fraction of correctly switched logic gates demonstrates that our results cannot be random events.

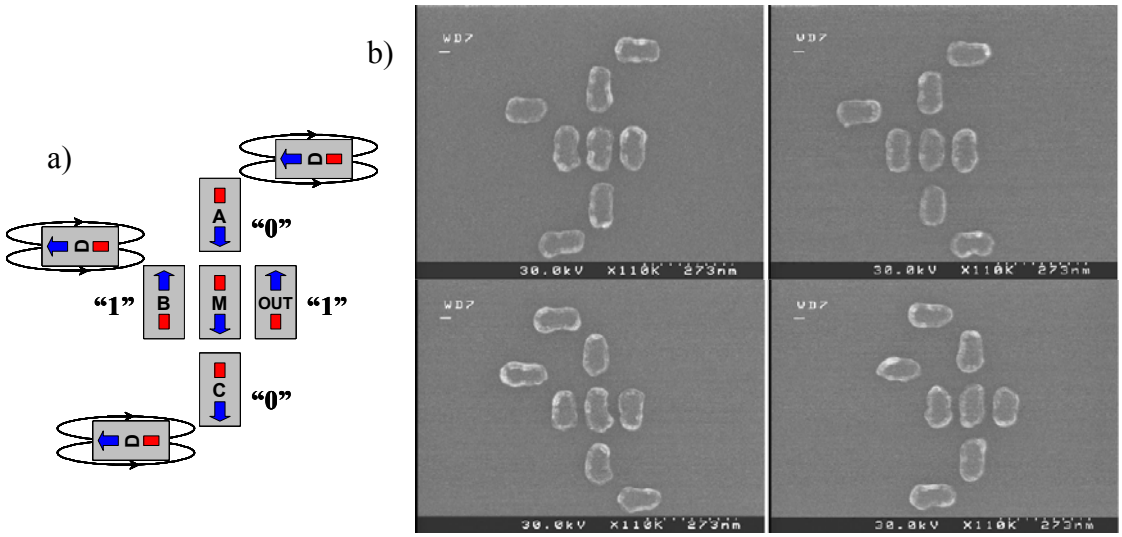

Figure 4. (a) Majority gate for MQCA. Horizontal nanomagnets labeled "D" are drivers that must be set by local magnetic fields provided by the inputs (b) Majority gates designed for testing all input combinations of the majority logic operation.

We believe that fabrication variations are responsible for yields less than 100% (22). Among those gates which showed proper switching, the run-to-run reliability was about 50%, meaning that about half of the nanomagnets were switching properly every time. We believe this effect was mostly due to clock-field misalignment between runs.

The three-input majority gate discussed above can be viewed as a programmable two-input NAND or NOR gate, depending on the state of any one of the three input magnets and accounting for inversion at the output magnet. Therefore, any Boolean logic function can be built by a network of majority gates. The inputs used in this work are set by the external clocking field and cannot be programmed independently; different combinations of the input values are realized by different physical arrangements of driver magnets. Nevertheless, the intersection of the horizontal and vertical wires, which is common to all structures, can correctly perform majority-logic functionality.

Demonstration of a majority gate combined with a binary wire

Here we present an experimental demonstration of a MQCA device that combines a majority gate with a binary wire. Figure 5 demonstrates final states after two sets of experiments in which a clocking field of 500 Oe with approximately 30 s rise and fall times (23) was applied in opposite directions along X axis. The magnetic force microscopy (MFM) data (24) in Fig. 5 show correct alignment of all magnetic dipoles of the gates.

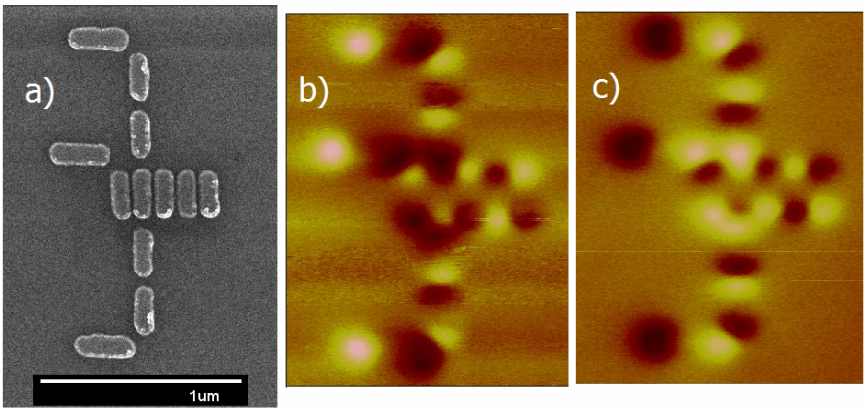

Figure 5. An MQCA device combining a majority logic gate with binary wires.
(a) Scanning electron microscope image and (b and c) magnetic force microscope images of magnetic ordering in the same gate for two orientations of horizontal clocking field. The nanomagnets deposited on silicon substrate are 40 nm thick and polycrystalline.

This example of "extended" majority gate brings up the question, how many nanomagnets can be contributed to the same switching process? We performed Monte Carlo simulations in the single-domain approximation to investigate whether the realization of larger-scale systems are feasible (26). Variations in nanomagnet shape and edge-roughness were taken into account in the distribution of the coupling fields at which switching occurs, i.e. switching fields (distribution of the demagnetization tensor elements), and thermal fluctuations were modeled by adding a stochastic field to the coupling field. We found that for our structures, the impact of switching field variations is far more important than the effect of thermal fluctuations. Strongly-coupled dots (sub 100 nm dot separation) fabricated by high-resolution lithography (with switching field variations less than 10 %) exhibit magnetic ordering over 10-20 magnets. This result agrees well with our previous experiments (27, 28) for samples fabricated by electron-beam lithography and lift-off. However, even with better fabrication technology, the number of nanomagnets that can be clocked together is limited. Therefore a larger-scale device would have to operate by means of local clocking of sub-arrays that realize a few gates only. The small number of magnets switching at the same time ensures that error levels can be kept acceptably small. This concept has been developed for EQCA (29). The most suitable architecture for adiabatically-clocked MQCA devices appears to be a pipelined structure. Because of the sequential arrangement of logic gates, there will inevitably be pipeline latency, however new data can be fed into the pipeline at each clock cycle. Clocking zones can be defined by locally applied clocking fields. Pipelined architectures are desirable in their own right due to their highly parallelized computing environment.

The minimum time necessary for magnetic switching is limited by magnetization precession in the nanomagnets and is on the order of 100 ps (25). The adiabatic pumping scheme further increases the clock-cycle time in MQCA devices by one or two orders of magnitude to eliminate precession from the switching process and to ensure predictable operation. Our simulations show that the majority gate reported here has an inherent

operating speed of 100 MHz and dissipation below 1 eV per switching event. As a worst-case estimate of the power dissipation in an MQCA system, at these speeds, and assuming that all nanomagnets switch in each clock cycle, 10^{10} gates would dissipate around a tenth of a watt.

Development of the input and readout for MQCA

Integration of MQCA elements with electronic circuitry will be possible in a manner similar to magnetic random access memories (MRAM) (30). Furthermore, integration of MQCA arrays into MRAM cells is also feasible, thus allowing the possibility of "intelligent memory" where the magnetic layer of an MRAM cell could not only store a single bit of information, but could also be capable of performing some basic logical processing. This may provide an opportunity to increase the functionality and integration density of an MRAM device.

A vital issue for any magnetic logic device is its ability to interact with outside electronics. Therefore the development of reliable interface converting electrical signals to magnetic fields, and magnetic fields back to electrical signals, remains crucial. Figure 6a shows a majority gate MQCA with attached inputs and outputs. The input-interfacing device, in principle, could be built using current carrying wires placed perpendicular to the input nanomagnets, in which case locally generated magnetic fields can switch the magnetization of the input nanomagnets. The output-interfacing device must non-invasively read the state of the MQCA logic gate and convert it to a measurable electrical signal. One possible candidate for the readout is based upon the resistance change in a magnetic wire caused by the trapping of a domain wall by the output nanomagnet in the MQCA circuit (Fig. 6b). We are currently investigating these options.

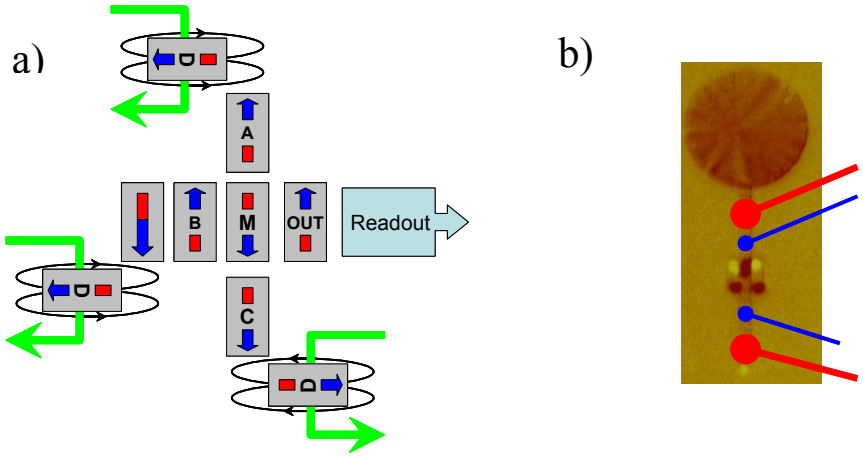

Figure 6. Interfacing MQCA. (a) Schematic representation of MQCA majority gate with input and output interface. Green lines represent current carrying wires generating local magnetic fields. (b) A possible implementation of a readout device. The MFM image shows a domain wall trapped in a magnetic wire between two nearby nanomagnets. Red and blue wires represent current and voltage carrying leads respectively. The structure is made of 40 nm thick permalloy, and the nanomagnets are separated from the wire by 60 nm.

Alternative fabrication techniques for MQCA fabrication

A very important issue for making MQCA viable is to eliminate fabrication errors that are presently limiting the size of the logic gates. The appropriate choice of fabrication technique should provide extremely dense arrays of precisely placed single-domain nanomagnets of uniform size and shape, and at the same time it should allow the custom design of various MQCA network layouts. The latter suggests the application of some kind of lithographic technique on the scale of the logic gates, while the requirement of highly uniform nanomagnets demands a true nanofabrication technique. Fortunately, our quest for MQCA technology may be able to follow the current developments in the hard disk drive (HDD) industry.

In order to further increase the areal density of HDDs, the classic continuous thin-film magnetic media will soon need to be replaced by a new technology (32). There are a few suggested technologies for this exchange, and one candidate is particularly interesting for us: it is patterned magnetic media. Here, the digital bits are stored as the magnetization of single-domain nanoelements, just as in the case of MQCA. Further similarity is that the nanomagnets are placed in regular arrays, and have strict requirement for uniformity. In patterned magnetic media, the HDD head addresses the nanomagnets one by one, which improves the signal to noise ratio of the read-write process as compared to the thin-film media, and thus enables the signal, i.e. the magnetization of the nanomagnets to be reduced. This leads to reduced volume, which ensures disk areal density over 40 Gb in^{-2}, possibly reaching to Tb in^{-2} (33). There are three excellent topical reviews published in the last six years addressing patterned magnetic media (30,33,34). These articles enumerate several different fabrication techniques that may be used and therefore are under development. The various techniques involve a group of the following processes: electron-beam lithography, X-ray and interference lithography, nanoimprinting, templated anodic oxidation of aluminum, or templated block-copolymer pattern formation, magnetic material deposition and pattern transfer. The deposition of the magnetic material is usually done by electroplating, sputter deposition or evaporation; and the pattern transfer applies reactive ion etching or low-energy ion irradiation. In addition to the conventional fabrication techniques, there is progress in guided self assembly of magnetic nanoparticles from colloidal solution.

There is a significant effort directed toward fabricating nanomagnets with an easy axis perpendicular instead of parallel to the surface, and fabrication of nanopillars, as well as patterning of metallic multilayers, which both provide out of plane magnetization orientation are presented.

Summary

In summary, we demonstrated the operation of the key elements for magnetic QCA computational architecture and that logic functions can also be realized in properly-structured arrays of physically-coupled nanomagnets. The technology for fabricating such nanometer scale magnets is currently under development by the hard disk drive industry.

While that latter work focuses entirely on data-storage applications, and physical coupling between individual bits is undesirable, our work points out the possibility of also realizing logic functionality in such systems, and indicates the potential of all-magnetic information processing systems that incorporate both memory and logic.

Acknowledgments

Our work is supported in part by grants from the Office of Naval Research, the W. M. Keck Foundation, and the National Science Foundation.

References

1. A. Ney, C. Pampuch, R. Koch, K. H. Ploog, *Nature*, **425,** 485 (2003).
2. R. P. Cowburn, M. E. Welland, *Science*, **287**, 1466 (2000).
3. D. A. Allwood et al., *Science*, **296**, 2003 (2002).
4. D. A. Allwood et al., *Science*, **309,** 1688 (2005).
5. G. Csaba, A. Imre, G. H. Bernstein, W. Porod, V. Metlushko, *IEEE Trans. Nanotechnol.,* **1,** 209 (2002).
6. C. S. Lent, P. D. Tougaw, W. Porod, G. H. Bernstein, *Nanotechnol.*, **4**, 49 (1993).
7. A. I. Csurgay, W. Porod, C. S. Lent, *IEEE Trans. Circ. Sys. –I.*, **47,** 1212 (2000).
8. G. Csaba, A. I. Csurgay, W. Porod, *Int. J. Circ. Theory Appl.,* **29**, 73 (2001).
9. G. Csaba, W. Porod, A. I. Csurgay, *Int. J. Circ. Theory Appl.*, **31**, 67 (2003).
10. A. O. Orlov, I. Amlani, G. H. Bernstein, C. S. Lent, G. L. Snider, *Science*, **277**, 928 (1997).
11. I. Amlani et al., *Science*, **284**, 289 (1999).
12. R. K. Kummamuru et al., *IEEE Trans. El. Dev.*, **50**, 1906 (2003).
13. A. O. Orlov et al., *Mesoscopic Tunneling Devices,* p.125, Research Signpost (2004).
14. G. L. Snider et al., *J. Appl. Phys.,* **85**, 4283 (1999).
15. C. S. Lent, *Science*, **288**, 1597 (2000).
16. G. Csaba, W. Porod, *J. Comput. El.*, **1,** 87 (2002).
17. V. P. Roychowdhury M. P. Anantram, *Journ. Appl. Phys.*, **85**, 1622 (1999)
18. M. C. B. Parish, M. Forshaw, *Appl. Phys. Lett.*, **83,** 2046 (2003).
19. S. A. Haque, M. Yamamoto, R. Nakatani, Y. Endo, *J. Magn. Magn. Mater.*, **282**, 380 (2004).
20. The micromagnetic simulations were performed using the Object Oriented Micromagnetic Framework (M. J. Donahue, D. G. Porter, OOMMF User's Guide, Version 1.0 Interagency Report NISTIR 6376, http://math.nist.gov/oommf/) of the National Institute of Standards and Technology.
21. A. Imre, G. Csaba, L. Ji, A. Orlov, G. H. Bernstein, and W. Porod, *Science*, **311**, 205 (2006).
22. Antiferromagnetic ordering was investigated in a large set of AFC lines designed to be identical. In a small percentage, we have found the ordering to fail even in the simplest, two-magnet systems. The identified faulty pairs performed highly repeatably, which indicates the errors to be related to fabrication variations. G. H. Bernstein et al., *Microelectr. Journ.,* **36**, 619 (2005).
23. The magnetizing process, i.e. the application of the clock-field, was performed in the homogenous field of an electromagnet capable of a maximum 7000 Oe. Due

to limitations imposed by the ramping rate of the generated field, the frequency of the clock-field was about 0.01 Hz in our experiments.
24. Magnetic force microscopy images were taken in a Digital Instruments Nanoscope IV with standard magnetic probes.
25. Th. Gerrits, H. A. M. van den Berg, J. Hohlfeld, L. Bar, Th. Rasing, *Nature*, **418,** 509 (2002).
26. G. Csaba, PhD thesis, University of Notre Dame (2003).
27. A. Imre, G. Csaba, G. H. Bernstein, W. Porod, V. Metlushko, *Proc. IEEE Nanotechnol.*, **2**, 20 (2003).
28. A. Imre, G. Csaba, G. H. Bernstein, W. Porod, V. Metlushko, *Superlatt. and Microstr.*, **34,** 513 (2003).
29. J. Timler, C. S. Lent, *Journ. Appl. Phys.*, **91**, 823 (2002).
30. C. A. Ross, *Annu. Rev. Mater. Res.*, **31**, 203 (2001).
31. J. M. Slaughter et al., *J. Supercon.*, **15**, 19 (2002).
32. D. A. Thompson and J. S. Best, *IBM Journ. Res. Develop.*, **44**, 311 (2000)
33. B. D. Terris and T Thomson, *Journ. Phys. D: Appl. Phys.*, **38**, R199 (2005).
34. J. I. Martin, J. Nogues, K. Liu, J. L. Vicent, and I. K. Schuller, *Journ. Magn. Magn. Mater.,* **256**, 449 (2003).